Astronomy & Astrophysics

Power-2 limb-darkening coefficients for the *uvby*, *UBVRIJHK*, SDSS *ugriz*, *Gaia*, *Kepler*, and TESS photometric systems

I. ATLAS stellar atmosphere models[⋆]

A. Claret[1,2] and J. Southworth[3]

[1] Instituto de Astrofísica de Andalucía, CSIC, Apartado 3004, 18080 Granada, Spain
  e-mail: claret@iaa.es
[2] Dept. Física Teórica y del Cosmos, Universidad de Granada, Campus de Fuentenueva s/n, 10871 Granada, Spain
[3] Astrophysics Group, Keele University, Staffordshire ST5 5BG, UK

ABSTRACT

Context. Limb darkening is an important stellar phenomenon and must be accounted for in the study of stellar spectra, eclipsing binaries, transiting planetary systems, and microlensing events. The power-2 limb-darkening law provides a good match to the specific intensities predicted by stellar atmosphere models: it is better than other two-parameter laws and is only surpassed by the four-parameter law.

Aims. Predictions of the limb-darkening coefficients for the power-2 law are not widely available. We therefore compute them, using stellar atmosphere models generated by the ATLAS (plane-parallel) code.

Methods. Limb-darkening coefficients were computed for the space missions *Gaia*, *Kepler*, and TESS as well as for the photometric systems *uvby*, *UBVRIJHK*, and SDSS *ugriz*. The calculations were performed by adopting the Levenberg–Marquardt least-squares minimisation method and were computed with a resolution of 100 equally spaced viewing angles. We used 9586 model atmospheres covering 19 metallicities, effective temperatures of 3500–50 000 K, $\log g$ values from 0.0 to 5.0, and microturbulent velocities of 0, 1, 2, 4, and 8 km s^{-1}.

Results. We confirm the superiority of the power-2 law, in terms of the quality of the fits, over other two-parameter laws. This is particularly relevant for the quadratic law, which is widely used.

Conclusions. We recommend the use of the power-2 law in cases where a two-parameter law is needed.

Key words. binaries close – binaries: eclipsing – planetary systems – stars: atmospheres

1. Introduction

The phenomenon of limb darkening (LD) is the apparent decrease in intensity of the surface of a star from the centre of its disc to the limb. The effect is not intrinsic to the star, but arises due to the viewing geometry of the observer. Viewing angles normal to the stellar surface experience photons emitted from deeper, and thus hotter, layers of the atmosphere, whereas the atmospheric opacity causes slanted viewing angles to 'see' only outer, and thus cooler, layers of the atmosphere.

The Sun has for centuries been known to show the phenomenon of LD (Bouguer 1760). It was first parameterised by the linear "law" (Schwarzschild 1906), which permits only a constant gradient in the decrease in surface brightness as a function of distance from the centre of the stellar disc:

$$\frac{I(\mu)}{I(\mu=1)} = 1 - u(1-\mu), \tag{1}$$

where I is the specific intensity of light as a function of position on the stellar disc, u is the linear limb-darkening coefficient (LDC), and $\mu = \cos\gamma$, where γ is the angle between the observer's line of sight and the surface normal.

The linear LD law is too simplistic, so many other LD parameterisations have been proposed. Some of the most widely used are the quadratic law (Kopal 1950),

$$\frac{I(\mu)}{I(\mu=1)} = 1 - a(1-\mu) - b(1-\mu)^2, \tag{2}$$

the square-root law (Díaz-Cordovés & Giménez 1992),

$$\frac{I(\mu)}{I(\mu=1)} = 1 - c(1-\mu) - d(1-\sqrt{\mu}), \tag{3}$$

and the logarithmic law (Klinglesmith & Sobieski 1970),

$$\frac{I(\mu)}{I(\mu=1)} = 1 - e(1-\mu) - f\,\mu\,\log(\mu), \tag{4}$$

where a, c, and e are the linear LDCs, b is the quadratic LDC, d is the square-root LDC, and f is the logarithmic LDC. The two-parameter laws provide an improved representation of reality as they allow for a slow drop-off of brightness near the centre of the stellar disc and a faster decrease in the region of the limb.

In addition to these, Hestroffer (1997) introduced a two-parameter law that involves a power of μ, which has become known as the power-2 law:

$$\frac{I(\mu)}{I(\mu=1)} = 1 - g(1-\mu^h), \tag{5}$$

---

where g and h are the corresponding LDCs. Here, it can be seen that the coefficient g gives the specific normalised intensity at the limb of the star ($\mu = 0$) and h governs how much the specific intensity departs from the linear law. The power-2 law has been found to fit specific intensity profiles very well (Morello et al. 2017; Maxted 2018) and has also been implemented in an efficient algorithm for planetary transits (Maxted & Gill 2019). Short et al. (2019) have shown that the power-2 law provides a better match to the specific intensities for spherical stellar atmosphere models than other two-parameter laws. To our knowledge, the only known LD law that surpasses it in quality of fit is the four-parameter law (Claret 2000).

Limb darkening is a vital phenomenon in several areas of astrophysics where a stellar disc is resolved in some way, including high-precision spectroscopy, eclipsing binary star systems, transiting extrasolar planets, interferometry, and stellar microlensing events. The power-2 law is beginning to be widely used in these areas.

Theoretical LDCs for the power-2 law have been presented for a subset of situations: DA, DB, and DBA white dwarfs (Claret et al. 2020), solar-type stars (Maxted 2018), and the passband of the CHEOPS space mission (Claret 2021). However, theoretical LDCs covering a wide range of stellar properties and passbands have not so far been available.

The aim of the current work is to provide users with LDCs for the power-2 law covering a wide range of stellar types and passbands (see Claret 2000; Claret & Bloemen 2011). The passbands are those for the Strömgren $uvby$, Johnson-Cousins $UBVRIJHK$, and SDSS $ugriz$ photometric systems, plus those for the *Gaia*, *Kepler*, and TESS space telescopes. In Sect. 2, we briefly describe the details of the computational method for deriving the LDCs adopting the ATLAS models. Sections 3 and 4 present the results of our calculations plus comparisons to the other two-parameter laws. We conclude in Sect. 5.

2. Numerical method

We adopted the least-squares method (LSM), adapted to the nonlinear case, to compute the LDCs. Before applying the LSM to each passband, the specific intensities for the $uvby$, $UBVRIJHK$, $ugriz$, *Gaia*, *Kepler*, and TESS photometric systems were integrated using the following equation:

$$I_a(\mu) = h^{-1} \frac{\int_{\lambda_1}^{\lambda_2} I(\lambda, \mu) S(\lambda) \lambda^{-1} \mathrm{d}\,\lambda}{\int_{\lambda_1}^{\lambda_2} S(\lambda) \mathrm{d}\,\lambda}, \tag{6}$$

where h is Planck's constant, λ is the wavelength, $I_a(\mu)$ is the specific intensity in passband a, $I(\lambda, \mu)$ is the monochromatic specific intensity, and $S(\lambda)$ is the response function. For the $uvby$, $UBVRIJHK$, and $ugriz$ passbands, the function also takes into account the transmission of one airmass of the Earth's atmosphere response. The passbands used were obtained from Spanish Virtual Observatory Filter Profile Service[1], except for the cases of Strömgren $uvby$, the passband of which was obtained from the Observatorio de Sierra Nevada, Granada, Spain (C. Cárdenas, priv. comm.), and JHK, obtained from the Observatorio del Teide-IAC, Spain (see also Alonso 1994).

The LDC calculations were performed adopting a total of 9586 ATLAS stellar model atmospheres[2]. These covered 19 metallicities [M/H] (from 10^{-5} to 10^{+1} times the solar

abundance), surface gravities log g from 0.0 to 5.0, effective temperatures T_{eff} from 3500 K to 50 000 K, and five microturbulent velocities ($V_\xi = 0, 1, 2, 4, 8 \, \mathrm{km \, s^{-1}}$). In each case, we used a total of 100 μ points equally spaced in μ, rather than the 17 points normally adopted in the ATLAS models.

The corresponding merit function to show the quality of the fit to the $I(\mu)$ values can be written as

$$\chi^2 = \sum_{i=1}^{N} (y_i - Y_i)^2, \tag{7}$$

where y_i is the model intensity at point i, Y_i is the fitted function at the same point, and N is the number of μ points.

3. Results and comparison with the quadratic law

The power-2 LDCs calculated in this work are made available in three tables (available at the CDS; see Table A.1). Table 1 contains the LDCs and χ^2 values for the *Gaia*, *Kepler*, and TESS passbands, Table 2 contains this information for the SDSS $ugriz$ bands, and Table 3 contains this information for the $uvby$ and $UBVRIJHK$ bands. The LDCs for the CHEOPS mission, computed using the ATLAS and PHOENIX models, can be found in Claret (2021).

Figure 1 illustrates the behaviour of the coefficients g and h for a series of models with differing T_{eff} and [M/H] values. It can be seen that the coefficient h does not depend very strongly on metallicity, except at low T_{eff}. The change in slope, around log $T_{\mathrm{eff}} = 3.9$, is due to the onset of convection. It can also be seen that coefficient h has little variation with T_{eff} or [M/H] in the interval $4.0 \leq \log T_{\mathrm{eff}} \leq 4.4$, staying within the range 0.5 to 0.4. This confirms a previous calculation of LDCs by Díaz-Cordovés et al. (1995), who found that the related square-root law works well at high T_{eff} values.

In this paper, we have focused our attention on a comparison between the power-2 and quadratic laws, as the quadratic one is by far the most widely used bi-parametric law. Figures 2 and 3 illustrate the behaviour of the normalised specific intensity near the limb of the star as a function of μ for the models with T_{eff} values of 4500 K and 23 000 K, respectively. The other input parameters are the same for both models: log $g = 5.0$, [M/H] = 0.0, and $V_\xi = 2 \, \mathrm{km \, s^{-1}}$. In both cases, the superiority of the power-2 law over the quadratic one is clear, mainly in the regions near the limb, where the differences in the normalised specific intensities can be of the order of 0.06. On the other hand, a comparison between Figs. 2 and 3 shows that the power-2 law works better for models with high T_{eff} values, mainly at the limb. We conducted tests with models with different input parameters, and the results are similar, although they vary slightly in relation to the previously mentioned values, depending on the region of the Hertzsprung–Russell diagram analysed.

A more general way of checking such differences in the quality of the fittings can be done by inspecting Figs. 4–8. These figures show the merit functions, χ^2, for the space missions *Gaia*, *Kepler*, and TESS. A direct comparison shows that the power-2 law (red asterisks) presents a much higher quality of fit than the corresponding quadratic one (black asterisks). However, we should recall that the two-parameter laws are accurate only for some regions of the Hertzsprung–Russell diagram. For example, for atmospheres in radiative equilibrium, the power-2 law works very well. However, for models in convective equilibrium (log $T_{\mathrm{eff}} \leq 3.85$), the power-2 law begins to present significant χ^2 values, albeit still much lower than in the case of the quadratic law.
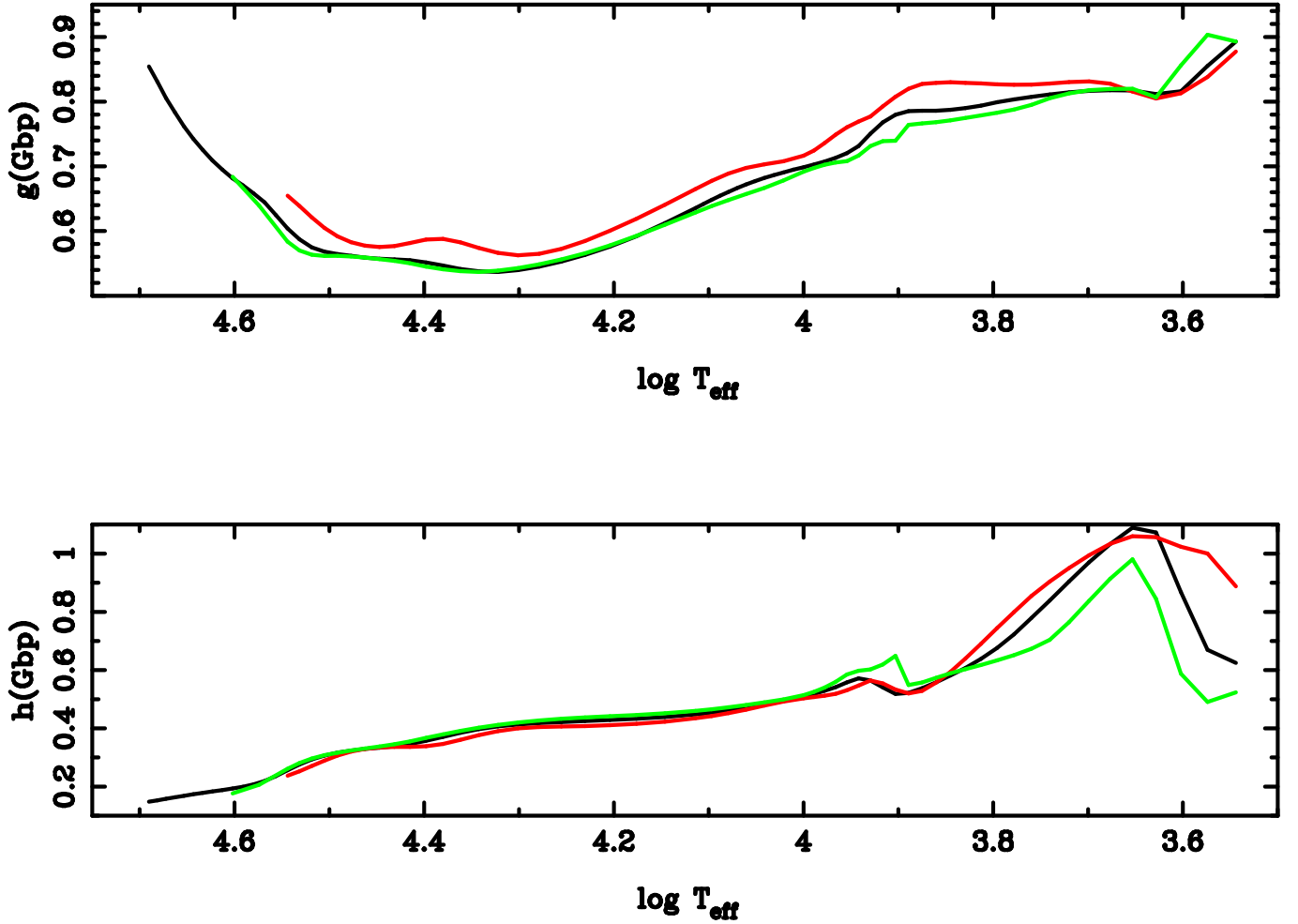

Fig. 1. Coefficients g and h for the filter Gbp of Gaia as a function of $T_{\rm eff}$ and [M/H]. Black lines represent [M/H] = 0.0, red lines [M/H] = 1.0, and green lines [M/H] = −1.0. In all cases, $\log g = 4.5$ and $V_\xi = 2$ km s^{-1}.
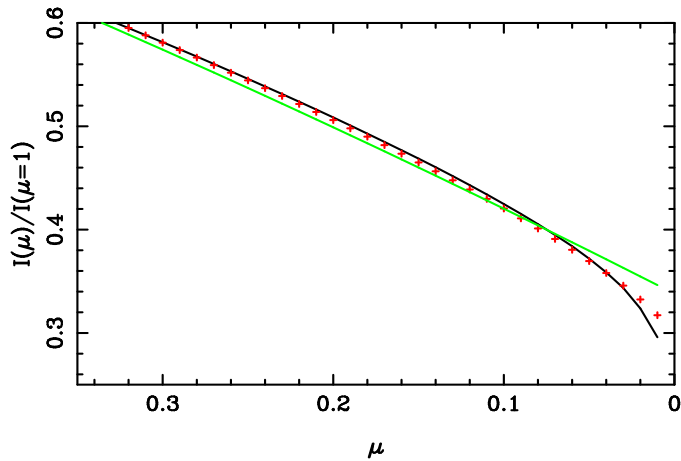

Fig. 2. Angular distribution of the specific intensity for a model with $T_{\rm eff} = 4500$ K, $\log g = 5.0$, [M/H] = 0.0, and $V_\xi = 2$ km s^{-1} for the TESS passband (black continuous line). Red crosses denote the fitting adopting the power-2 law, and the green line represents the quadratic LD law approach.
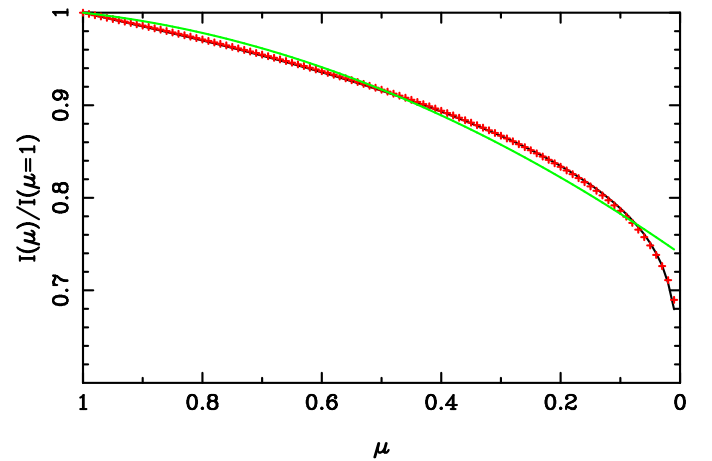
Fig. 3. Same as Fig. 2 but for the model with $T_{\rm eff} = 23\,000$ K, $\log g = 5.0$, [M/H] = 0.0, and $V_\xi = 2$ km s^{-1}.

4. Comparison with the square-root and logarithmic laws

For completeness, we also compared the quality of fit for the power-2 law with those computed by adopting the square-root

and logarithmic LD laws. These are rarely used in the analysis of transiting planets but are often used in the study of eclipsing binary systems (e.g. Van Hamme 1993).

Figure 9 shows a comparison of the merit functions for the G passband using the square-root law (black asterisks) and the power-2 (red asterisks). We have kept the same scale to facilitate a comparison with the results shown in Fig. 5. It can be
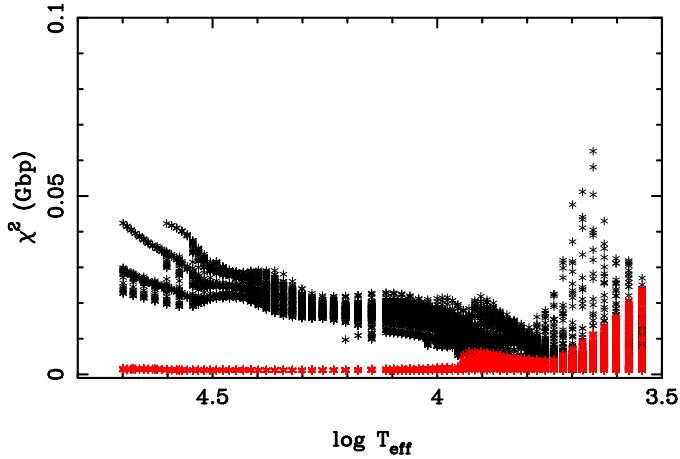
Fig. 4. Merit function for the ATLAS models as a function of $\log T_{\mathrm{eff}}$ for the *Gaia* G_{BP} passband. The power-2 law is shown using red asterisks and the quadratic law using black asterisks. The results for all models are shown.

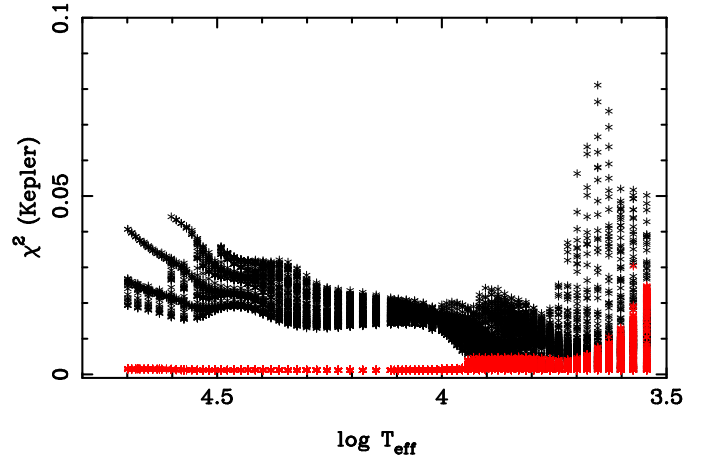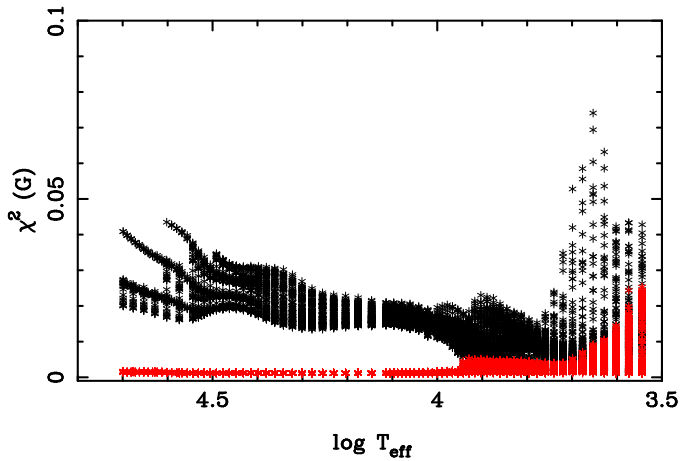**Fig. 5.** Same as Fig. 4 but for the *Gaia G* passband.
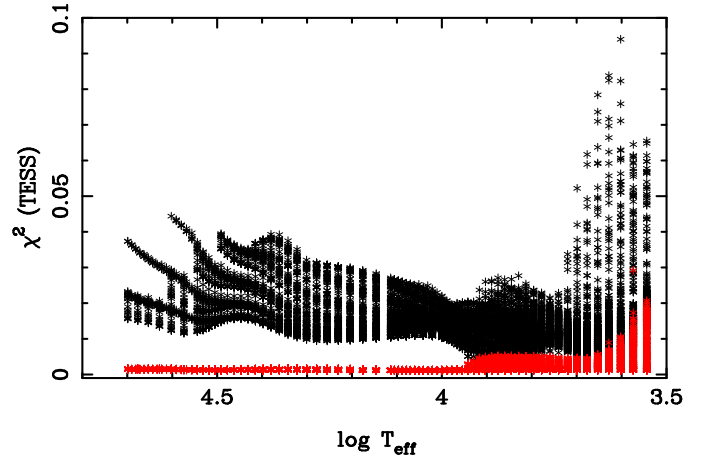

Fig. 6. Same as Fig. 4 but for the *Gaia G_{RP}* passband.

Fig. 7. Same as Fig. 4 but for the *Kepler* passband.

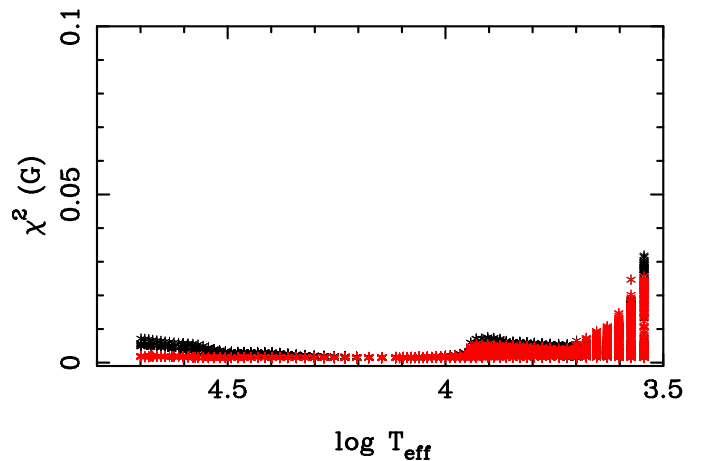**Fig. 8.** Same as Fig. 4 but for the TESS passband.

Fig. 9. Same as Fig. 5 but for the square-root law (black asterisks) versus the power-2 law (red asterisks).

seen that the superiority of the fits provided by the power-2 law (Fig. 9) is not as great as for the quadratic law (Fig. 5) because the square-root law is a better representation than the quadratic law. In fact, Díaz-Cordovés & Giménez (1992) have shown that the values of σ for the square-root law are of the order of ten times smaller than those provided by the quadratic one. To assess the quality of a fit, Díaz-Cordovés & Giménez (1992) used a definition of the merit function slightly different from the one given by Eq. (7):

$$\sigma^2 = \frac{1}{N} \sum_{i=1}^{N} (y_i - Y_i)^2 \,, \tag{8}$$

where N, y_i, and Y_i have the same meaning as in Eq. (7).
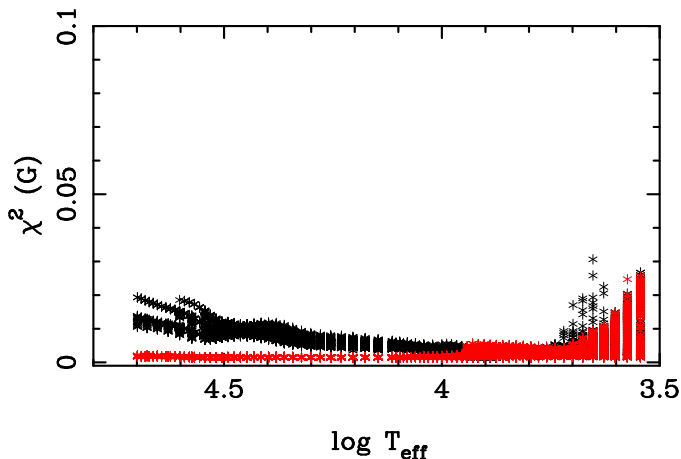
Fig. 10. Same as Fig. 5 but for the logarithmic law (black asterisks) versus the power-2 law (red asterisks).

Figure 10 shows the same comparison but for the logarithmic law. It can be seen that the logarithmic law provides a better fit to the model atmosphere intensities than does the quadratic law (Fig. 5), but it is clearly inferior to the square-root (Fig. 9) and power-2 laws. This conclusion holds particularly at higher T_{eff} values, as the logarithmic law performs relatively well for $5500 < T_{eff} < 9000$ K. In summary, in addition to the fact that Eq. (5) is a non-linear law, as noted by Hestroffer (1997), it exhibits steeper $\frac{\partial I}{\partial \mu}$ gradients at the limb (see, for example, Figs. 2 and 3). This makes it the bi-parametric law that best fits the distribution of intensities from atmosphere models, as we have seen by inspecting Figs. 4–10.

5. Summary

The power-2 LD law is seeing increasing use in several areas of stellar physics. In order to help this work, we have calculated LDCs for the power-2 law using ATLAS model atmospheres covering a wide range of stellar T_{eff} values, gravities, and metallicities. This has been done for a large number of passbands used by both ground-based and space-based telescopes.

In addition to the LDCs, we have calculated the quality of fit to the specific intensities from the model atmospheres. A comparison between these and other two-parameter LD laws shows that the power-2 law produces the best results in all cases, followed by the square-root and logarithmic laws. The quadratic law is by far the worst of the four options. The differences between the χ^2 provided by the power-2 law and the quadratic one are particularly important for regions near the limb and for low T_{eff} values, and can reach more than one order of magnitude. We find similar results for comparisons in all of the passbands considered. Additional calculations for other photometric systems and/or the transmissions of the filters and the response of the Earth's atmosphere are available upon request.

Therefore, we recommend the power-2 law to users who prefer to use a two-parameter LD law. We note that the four-parameter law provides a better fit, particularly in the cases of eclipsing binaries and extrasolar planet transits with stars that have low T_{eff} values. For the specific case of short-period eclipsing binaries, it would also be advisable to take the mutual irradiation into account because it can significantly alter both the corresponding LDCs and the bolometric albedo. In fact, irradiated stellar atmospheres show different distributions of brightness if we compare them with standard models without the action of an external radiation field. More details on this matter are available in Claret (2001, 2004) and Claret & Giménez (1992).

References

Alonso, A., Arribas, S., & Martínez-Roger, C., 1994, A&AS, 107, 365
Bouguer, P., 1760, Traité d'Optique, l'Abbé de la Caille, Paris
Claret, A., 2000, A&A, 363, 1081
Claret, A., 2001, MNRAS, 327, 989
Claret, A., 2004, A&A, 422, 665
Claret, A., 2021, RNAAS, 5, 13
Claret, A., & Bloemen, S. 2011, A&A, 529, A75
Claret A., & Giménez A. 1992, A&A, 256, 572
Claret, A., Cukanovaite, E., Burdge, K., et al. 2020, A&A, 634, A93
Díaz-Cordovés, J., & Giménez, A. 1992, A&A, 259, 227
Díaz-Cordovés, J., Claret, A., & Giménez, A. 1995 A&AS, 110, 329
Hestroffer, D. 1997, A&A, 327, 199
Klinglesmith, D. A., & Sobieski, S. 1970, AJ, 75, 175
Kopal, Z. 1950, Harvard Coll. Observ. Circ., 454, 1
Kopal, Z. 1959, Close Binary Systems (London: Chapman & Hall)
Maxted, P. F. L. 2018, A&A, 616, A39
Maxted, P. F. L., & Gill, S. 2019, A&A, 622, A33
Morello, G., Tsiaras, A., Howarth, I. D. et al. 2017 AJ, 154, 111
Schwarzschild, K. 1906, Nachrichten von der Gesellschaft der Wissenschaften zu Göttingen, Mathematisch-Physikalische Klasse, 43
Short, D. R., Welsh, W. F., Orosz, J. A., et al. 2019, RNAAS, 3, 117
Van Hamme, W. 1993, AJ, 106, 2096

Appendix A: Description of Tables 1-3 (available at the CDS)

Table A.1. Power-2 LDCs for the *Gaia*, *Kepler*, TESS, SDSS Sloan *ugriz* and *uvby UBVRIJHK* photometric systems.

Name	Source	T_{eff} values (K)	log g (c.g.s.)	[M/H] (dex)	V_ξ (km s^{-1})	Photometric system	Fit/equation
Table1	ATLAS	3500 – 50000	0.0 – 5.0	−5.0 – 0.0	0, 1, 2, 4, 8	*Gaia*, *Kepler*, TESS	LSM/Eq. 5
Table2	ATLAS	3500 – 50000	0.0 – 5.0	−5.0 – 0.0	0, 1, 2, 4, 8	SDSS Sloan *ugriz*	LSM/Eq. 5
Table3	ATLAS	3500 – 50000	0.0 – 5.0	−5.0 – 0.0	0, 1, 2, 4, 8	*uvbyUBVRIJHK*	LSM/Eq. 5